PCCP

Accepted Manuscript




ROYAL SOCIETY OF CHEMISTRY

www.rsc.org/pccp

Cite this: DOI: 10.1039/c0xx00000x

www.rsc.org/xxxxxx

ARTICLE TYPE

# On the Structure of Ce-containing Silicophosphate Glasses: a Core-Shell Molecular Dynamics Investigation.

**Elisa Gambuzzi [a] and Alfonso Pedone*[a]**

***Received (in XXX, XXX) Xth XXXXXXXXX 20XX, Accepted Xth XXXXXXXXX 20XX***

**DOI: 10.1039/b000000x**

Classical molecular dynamics simulations have been used to investigate the local and medium range structure of Ce-containing silicophosphate glasses widely used in optical and photonic devices because of their enhanced UV absorption and radiation damage resistance properties. New $Ce^{3+}$-O and $Ce^{4+}$-O parameters for a force-field based on the core-shell model were developed by fitting on the crystalline structures of Ce-containing crystal phases, and used to get insights into the structure of five silicophosphate glasses with increasing $Ce_2O_3$ and $P_2O_5$ content. An excellent agreement between experimental and computational data was found for the local environment around cerium ions and network former cations. $Ce^{3+}$-O bond lengths are generally longer than $Ce^{4+}$-O, which shows higher coordination numbers. Both P and Si are four-fold coordinated; their allocation in the network is not uniform: the increasing in Ce content leads to the formation of silica-rich domains and phosphate-rich domains, which entrap Ce cations increasing their solubility in the glass. We found that both the $Q^n$ distributions of phosphorous and Ce clustering depend on the Ce/P ratio in the glass. In particular, Ce clustering begins for Ce/P ratios between 0.17 and 0.29 in the glass series investigated.

## Introduction

Cerium-containing materials are widely used in optical and photonic devices such as optical windows, laser, and optical amplifiers[1, 2]. Since cerous ($Ce^{3+}$) and ceric ($Ce^{4+}$) ions absorbs at 240 and 314 nm, they provide matrices with enhanced UV absorption and transparency in the visible spectral area. Instead, in case of ionizing-radiation exposure, $Ce^{3+}$ acts as traps of holes and $Ce^{4+}$ as traps of electrons, activating a radiation-resistance mechanism that prevents the overall worsening of the optical properties of the glass.[3-5] Moreover, in the last decade the antioxidant properties of $Ce^{3+}$ ions have been also exploited in the field of silica-based bioactive glasses[6]. Ce-doping is thus an interesting procedure that improves optical and biological performances of Ce-containing materials.

Unfortunately, Cerium, like other Rare-Earth (RE) ions, shows very low solubility in pure silica[7, 8], where it tends to form clusters through RE-O-RE bridges.[9] The solubility of RE ions increases in alkali silicate glasses, since the addition of alkaline modifiers (such as Li, Na, K, etc.) leads to a more depolymerized silica network, where regions rich in non-bridging oxygens (NBOs) can bind RE ions.[10] In fact, ternary homogenous $SiO_2$-$Na_2O$-$RE_2O_3$ glasses can be synthesized.[11, 12]

The addition of aluminum has also been shown to effectively disperse the RE ions in $SiO_2$-$Al_2O_3$-$RE_2O_3$ glasses[13, 14] because the exceeding negative charge carried by the $[AlO_4]^-$, $[AlO_5]^{2-}$, and $[AlO_6]^{3-}$ polyhedra formed depending on the $RE_2O_3$ content, balances the charge of RE cations increasing their solubility.[15, 16]

Another effective solution to increase the RE solubility in silicate matrices is that of adding $P_2O_5$. In fact, the $Q^n$ species of phosphorous (where Q stands for quaternary species connected to *n* bridging oxygens (BO), $n$ = 1, 2 or 3, depending on the RE content[17, 18]) act as a solvation shells around the RE ions, separating them from the silicon-oxygen network.[14, 19]

Understanding the structure of silicophosphate glasses and the relation between the glass composition and RE clustering has thus become fundamental to design new RE-containing matrices with desired optical properties since the presence of Ce-O-Ce clusters is associated to the loss of visible light transparency of glasses.[20-23]

In the particular case of Ce-containing glasses, the literature is quite rich of works focused on the characterization of their optical properties[20-23] but few studies focused on their structure. To the best of our knowledge, only two works, one

**Table 1** Shell model interatomic potential parameters. Atomic charges are reported as superscript text; "Oh" refers to Oxygen atoms bonding Hydrogen atoms.

| | References | | | |
|---|---|---|---|---|
| | | | Buckingham | |
| | | $A_{ij}$ (eV) | $\rho_{ij}$ (Å) | $C_{ij}$ (eV Å$^6$) |
| $O_s^{-2.8482}$-$O_s^{-2.8482}$ | 28 | 22764.30 | 0.1490 | 27.88 |
| $Oh_s^{-2.3}$-$Oh_s^{-2.3}$ | 54 | 22764.30 | 0.1490 | 6.97 |
| $Oh_s^{-2.3}$-$H^{+1.4}$ | 43 | 311.97 | 0.25 | 0.0 |
| $Si^{4+}$-$O_s^{-2.8482}$ | 28 | 1283.91 | 0.32052 | 10.66158 |
| $Al^{3+}$-$O_s^{-2.8482}$ | 36 | 1460.3000 | 0.29912 | 0.0 |
| $Al^{3+}$-$Oh_s^{-2.3}$ | 41 | 1142.6775 | 0.29912 | 0.0 |
| $P^{5+}$-$O_s^{-2.8482}$ | 38 | 1120.0913 | 0.334772 | 0.0 |
| $Ce^{3+}$-$O_s^{-2.8482}$ | this work | 2893.340501 | 0.323317 | 0.0 |
| $Ce^{4+}$-$O_s^{-2.8482}$ | this work | 45241.636456 | 0.306140 | 0.0 |
| | | | Three-body potential | |
| | | $k_b$ (eV rad$^{-2}$) | $\theta_0$ (deg) | $\rho$ (Å) |
| $O_s^{-2.8482}$-$Si^{4+}$-$O_s^{-2.8482}$ | 28 | 100.0 | 109.47 | 1.0 |
| $O_s^{-2.8482}$-$P^{5+}$-$O_s^{-2.8482}$ | 39 | 50.0 | 109.47 | 1.0 |
| $P^{5+}$-$O_s^{-2.8482}$-$P^{5+}$ | 38 | 50.0 | 141.18 | 1.0 |
| | | | Core-shell spring potential | |
| | | $k_{c\text{-}s}$ (eV Å$^{-2}$) | Y(e) | |
| $O_c^{+0.8482}$-$O_s^{-2.8482}$ | 37 | 74.92 | -2.8482 | |
| $Oh_c^{+0.9}$-$Oh_s^{-2.3}$ | 43 | 74.92 | -2.3000 | |
| | | | Morse potential | |
| | | $D_{ij}$(eV) | $\beta_{ij}$ (Å$^{-1}$) | $r_{ij}^0$(Å) |
| $Oh^{-2.3}$-$H^{+1.4}$ | 43 | 7.05250 | 3.1749 | 0.9485 |

experimental and one computational, extensively investigated both short-range and medium-range order of Ce-containing silicophosphate glasses.

In 2011, Rygel et al.[24] used X-ray techniques to study Ce environment in a series of 9 aluminophosphate and 8 silicophosphate glass compositions. Their work provided precious reference experimental data on the Ce oxidation state, Ce coordination number and estimation of Ce clustering in glass matrixes. In particular, the XPS results showed that, for glasses melted in air, more than 95% of cerium ions are $Ce^{3+}$ whereas EXAFS experiments provided an average Ce coordination number of ~7.0 with an average cerium-oxygen bond length of 2.41 Å. Moreover, Ce clustering was suggested based on numerical calculations for silicophosphate glasses containing more than 15 mol% $Ce_2O_3$.

Recently, Du et al.[19] investigated the $Ce^{3+}$ and $Ce^{4+}$ structural environment in one silicophosphate, one aluminophosphate and one aluminosilicophosphate glass by means of classical molecular dynamics (MD) simulations based on a rigid ionic (RI) force-field. To validate the force field, they referred to Rygel et al.[14, 24] experimental data, even though the glass composition employed in the two works were not exactly the same. Du et al.[19] found a longer Ce-O bond length and larger coordination number for $Ce^{3+}$ than for $Ce^{4+}$ (2.48 and 6.4 vs. 2.24 and 5.8, respectively). Moreover, the silica network of the cerium silicophosphate glass was highly polymerized and dominated by $Q^4$ species, with 5% of Si ions coordinated by 5 oxygens. In agreement with previous experimental hypothesis,[14] cerium ions were found to be preferentially surrounded by $PO_4$ tetrahedra, which form a kind of solvation shell around them.

The RI force fields are accurate in describing the short-range structural order of oxide glasses,[25] but it has been shown in several works that they do not perform equally well in describing medium-range features[26-28] such as network depolymerization, $Q^n$ distributions of former cations, network chemical and topological disorder, and extra-framework cation clustering.

With respect to the RI model, the core-shell (CS) model[29] allows a straightforward treatment of the polarizability of ions necessary to deeply relax the network glass structures during quenching,[27] and, thus better reproduces the medium-range structure of glasses.[26, 28]. Unfortunately, although two sets of core-shell interatomic potential parameters for the $Ce^{3+}$-O and $Ce^{4+}$-O pairs are present in the literature[34, 35], they cannot be used to simulate Ce-containing silicophosphate glasses, being not consistent with Si/P-O potential parameters available in literature.[28] The oxygen parameters (charge splitting and the harmonic force constant between core and shell) of these potentials are very different to the one previously developed for silicate and/or phosphate phases.[28]

It is worth to highlight that other classical potential allow an explicit treatment of ion polarizability, like the aspherical ion model (AIM)[30, 31] and the polarizable ion model (PIM)[32, 33], but they do not contain all the parameters of the atomic pairs to which we are interested at the moment. They could certainly be exploited in the future.

In this work, we will extend a core-shell model force field[28] successfully employed in the past for the simulations of alkali and alkaline earth silicate, phosphosilicate, aluminosilicate glasses[26, 28, 32, 36-40] and phosphate glasses[26, 28, 32-37] to Ce-containing silicophosphate glasses.

**Table 2** Composition (mol%) of the investigated glasses, number of atoms ($N_{TOT}$) per simulation box and density before (Priven) and after NPT relaxation.

| | CSP2 | CSP3 | CSP4 | CSP6 | CSP9 | CSP |
|---|---|---|---|---|---|---|
| $Ce_2O_3$ (mol%) | 2.2 | 4.1 | 7.5 | 18.2 | 23.8 | 8.0 |
| $P_2O_5$ (mol%) | 34.6 | 38.6 | 44.9 | 62.1 | 72.7 | 37.0 |
| $SiO_2$ (mol%) | 60.9 | 54.9 | 45.6 | 17.4 | 0.7 | 55.0 |
| $Al_2O_3$ (mol%) | 2.3 | 2.4 | 2.0 | 2.3 | 2.8 | 0.0 |
| $N_{TOT}$ | 5010 | 5001 | 5005 | 5012 | 5301 | 5422 |
| Priven density [g·cm$^{-3}$] | 2.539 | 2.655 | 2.833 | 3.302 | 3.357 | 2.716 |
| NPT density [g·cm$^{-3}$] | 2.501 | 2.612 | 2.734 | 3.148 | 3.193 | --- |

To validate the newly developed parameters, we simulated the structure of several Ce-containing silicate and phosphate crystals, and of five silicophosphate glasses with variable Ce/P ratio, and $Ce_2O_3$ content. The structures obtained will be compared with the available experimental data on Ce environment provided by Rygel et al.[24] for silicophosphate glasses. The $Ce^{3+}$ and $Ce^{4+}$ environment as well as the short- and medium-range order of each cation, will be thoroughly investigated in order to provide insights on Ce-containing silicophosphate glass structures.

## Methods

### Force field potential form

The adopted force field was built accordingly to the Born model, which assumes that ions interact via long-range electrostatic forces and short-range forces.

The interaction between two ions, *i* and *j*, are expressed through the Buckingham potential combined with the electrostatic energy:

$$U(r_{ij}) = k\frac{q_i q_j}{r_{ij}} + A_{ij}e^{-\left(\frac{r_{ij}}{\rho_{ij}}\right)} - \frac{C_{ij}}{r_{ij}^6} \qquad (1)$$

in which, $A_{ij}$, $\rho_{ij}$ and $C_{ij}$ are the parameters to be fitted, while $q_i$ and $q_j$ are the charges of ions which have been fixed to the formal charges, k is $1/4\pi\varepsilon_0$ (where $\varepsilon_0$ is the dielectric constant) and $r_{ij}$ is the distance between atoms *i* and *j*. The Coulomb forces act between all species whereas the Buckingham function models the Si–O, P–O, Al–O and Ce–O short range interactions.

Oxygen ions are modelled by the shell-ion model potential of Dick and Overhauser[29]: the total ionic charge Z is shared among a massless shell of charge -Y, on which all short range forces act, and a core of charge Z+Y, which are coupled by a harmonic spring potential of the form:

$$U(r_{c-s}) = \frac{k_{c-s}}{2}(r_{c-s})^2 \qquad (2)$$

where $k_{c-s}$ is the core–shell spring constant and $r_{c-s}$ is the distance between the core and the shell.

A three-body screened harmonic potential is used to control the intra-tetrahedral O-Si-O and O-P-O and P-O-P angles

$$U(\theta_{ijk}) = \frac{k_b}{2}(\theta_{ijk} - \theta_{ijk}^0)^2 \cdot e^{\left(-\frac{r_{ij}}{\rho}-\frac{r_{ik}}{\rho}\right)} \qquad (3)$$

Where $k_b$ is the three-body force constant, $\theta_{ijk}$ is the angle between atoms *i*, *j* and *k* and $\theta_{ijk}^0$ is the reference angle between atoms *i*, *j* and *k*. $r_{ij}$ is the distance between *i* and *j*, a $r_{ik}$ is the distance between *i* and *k*, and ρ is a parameter. Finally, the Morse function describes the O-H bond of hydroxyl groups present in one of the crystal phases used to validate the developed force-field parameters (*vide infra*).

$$U(r_{ij}) = D_{ij}\left[\left(1 - e^{-\beta_{ij}(r_{ij}-r_{ij}^0)}\right)^2\right] \qquad (4)$$

Table 1 lists all the force field parameters used in this work. It is worth to highlight that we derived, for the first time, a set of Buckingham parameters $A_{ij}$, $\rho_{ij}$ and $C_{ij}$ for the $Ce^{3+}$-$O_s$ and $Ce^{4+}$-$O_s$ atom pairs, which are consistent with the most common core-shell force field employed in the simulation of silica-based glasses. The parameters for the Si-$O_s$, P-$O_s$, Al-$O_s$, Oh-Oh, $O_s$-$O_s$, Al-Oh, Oh-H pairs and $O_s$-Si-$O_s$, $O_s$-P-$O_s$, P-$O_s$-P three-body terms were taken from the literature. [26, 28, 37-39, 41-43] $Ce^{3+}$-$O_s$ and $Ce^{4+}$-$O_s$ Buchingham parameters were fit, initially, on the crystalline structures of $Ce_2O_3$ oxide[44] and $CeO_2$ oxide[45], respectively. Subsequently, the parameters were refined on further 5 structures: $CeP_5O_{14}$,[46] $Ce_2Si_2O_7$,[47] $CePO_4$,[48] Ce-florencite ($Al_3CeP_2O_{14}H_6$) [49] and $CeSiO_4$ [50] crystal phases. The relaxed fitting procedure encoded in the GULP software was used [51, 52].

No three-body potential was imposed on the $O_s$-Al-$O_s$ bond angle to guide tetrahedral coordination. Indeed, the small amount of $Al_2O_3$ in the glass compositions under study, and the absence of other network modifier oxides but $Ce_2O_3$ at low-medium concentration, make Al itself act as a network modifier, with an average coordination number varying from 5 to 6.[53]

### Generation of the models and structural analysis

Five of the Ce-silicophosphate (CSP) glasses experimentally investigated by Rygel et al.[24] were simulated: CSP2, CSP3, CSP4, CSP6 and CSP9, for which the $Ce_2O_3$ oxide content varies from 2.2 to 23.8 % mol, the $P_2O_5$ content increases from 34.6 to 72.7 mol%, the $SiO_2$ content decreases from 60.9 to 0.7 mol%, whereas the $Al_2O_3$ content remains constant around 2.0-2.8 mol%. Moreover, the CSP composition investigated by Du et al.[19] was also simulated in order to compare the $Q^n$ distributions calculated by both rigid ion and core-shell models. The compositions of the investigated glasses, as well as the total number of atoms in the MD models and densities are reported in Table 2. For each composition, we generated three models of about 5000 atoms. The $Ce^{4+}/Ce^{3+}$ ratio was fixed accordingly to experimental findings ($[Ce^{4+}] \leq 3\%$ of Ce atoms)[24] for CSP6 and CSP9 glasses. However, we chose slightly higher $Ce^{4+}/Ce^{3+}$ ratios for CSP2 (6.5 %) and CSP3 (3.5 %), in order to have a better statistics for $Ce^{4+}$ ions. However, it is worth to highlight that because of the small number of $Ce^{4+}$ ions present in the CSP2, CSP3 and CSP4 glasses, only the structural data regarding $Ce^{4+}$ environment for the CSP6 and CSP9 glasses will be reported.

**Table 3** Unit cell parameters and Ce-O bond lengths of crystalline phases before (experimental structure), and after (**bold** text) an isobaric geometry optimization run with the force field presented in this work. The results obtained by using the RI model proposed by Du et al.[19] are also reported for comparison (*italic* text).

| Phase | Space group | a / b / c | V [Å$^3$] | ΔV%[(a)] | <Ce-O> [Å][(b)] | Ce-O [Å][(b),(c)] |
|---|---|---|---|---|---|---|
| | | | $Ce^{3+}$ | | | |
| $Ce_2O_3$ | P $\bar{3}$m1 | 3.891/3.891/6.059 | 79.443 | | (1) 2.50 | (1) 2.34$^3$/2.69$^3$/2.43 |
| | | **3.888/3.888/6.063** | **79.365** | **-0.10** | **2.50** | **2.31$^3$/2.69$^3$/2.52** |
| | | *3.898/3.898/5.9701* | *78.555* | *-1.12* | *2.50* | *2.32$^3$/2.67$^3$/2.52* |
| $CeP_5O_{14}$ | P 1 | 9.227/8.891/7.219 | 541.309 | | 2.48 | 2.39/2.42/2.45/2.49/2.50/2.54/2.55 |
| | | **9.259/9.009/7.249** | **546.122** | **+0.89** | **2.43** | **2.36/2.37/2.42/2.43/2.45/2.46/2.50** |
| | | *9.165/8.626/7.366* | *535.469* | *-1.08* | *2.52* | *2.43/2.44/2.45/2.50/2.56/2.64/2.65* |
| | | | | | 2.46 | 2.40//2.40/2.45/2.47/2.49/2.51/2.52 |
| | | | | | **2.42** | **2.37/2.38/2.38/2.41/2.45/2.45/2.47** |
| | | | | | *2.48* | *2.35/2.36/2.43/2.44/2.48/2.62/2.71* |
| $Ce_4(Si_2O_7)_2$ | P 41 | 6.796/6.796/24.728 | 1142.222 | | 2.53 | 2.42/2.45/2.48/2.52/2.55/2.55/2.72 |
| | | **6.849/6.849/25.223** | **1183.300** | **+3.60** | **2.55** | **2.39/2.44/2.46/2.51/2.52/2.57/2.96** |
| | | *6.903/6.903/25.246* | *1202.946* | *+5.32* | *2.56* | *2.36/2.36/2.49/2.50/2.51/2.55/3.12* |
| | | | | | 2.54 | 2.38/2.43/2.52/2.54/2.60/2.64/2.67 |
| | | | | | **2.55** | **2.31/2.42/2.48/2.57/2.58/2.69/2.83** |
| | | | | | *2.54* | *2.34/2.48/2.52/2.53/2.54/2.57/2.80* |
| | | | | | 2.48 | 2.36/2.37/2.38/2.45/2.50/2.60/2.67 |
| | | | | | **2.49** | **2.31/2.35/2.36/2.47/2.50/2.57/2.90** |
| | | | | | *2.50* | *2.31/2.40/2.41/2.42/2.54/2.58/2.85* |
| | | | | | 2.53 | 2.42/2.45/2.46/2.46/2.48/2.54/2.67 |
| | | | | | **2.52** | **2.41/2.41/2.45/2.47/2.47/2.52/2.90** |
| | | | | | *2.52* | *2.39/2.41/2.41/2.43/2.44/2.55/3.04* |
| $CePO_4$ | P 2$_1$ / n | 6.790/7.020/6.292 | 299.928 | | (1) 2.51 | (1) 2.45/2.46/2.48/2.53/2.53/2.57/2.58 |
| | | **6.815/6.947/6.753** | **308.372** | **+2.82** | **2.53** | **2.41/2.41/2.44/2.55/2.61/2.63/2.63** |
| | | *6.760/6.951/6.845* | *311.554* | *+3.88* | *2.57* | *2.46/2.51/2.51/2.52/2.59/2.69/2.69* |
| $Al_3CeP_2O_{14}H_6$ | R $\bar{3}$m | 6.764/6.764/6.764 | 228.451 | | (1) 2.66 | (1) 2.72$^2$/2.65$^6$ |
| | | **6.931/6.931/6.931** | **234.378** | **+2.59** | **2.62** | **2.75$^2$/ 2.58$^6$** |
| | | | $Ce^{4+}$ | | | |
| $CeO_2$ | F m3m | 3.826/3.826/3.826 | 39.607 | | (1) 2.34 | (1) 2.34$^8$ |
| | | **3.851/3.851/3.851** | **40.376** | **+1.94** | **2.34** | **2.34$^8$** |
| | | *3.846/3.846/3.846* | *40.231* | *+1.58* | *2.36* | *2.36$^8$* |
| $CeSiO_4$ | I 41/amd | 6.956/6.956/6.195 | 299.800 | | (1) 2.32 | (1) 2.27$^4$/2.36$^4$ |
| | | **6.892/6.892/6.297** | **299.156** | **-0.22** | **2.34** | **2.26$^4$/2.42$^4$** |
| | | *6.904/6.904/6.273* | *298.981* | *-0.27* | *2.37* | *2.28$^4$/2.45$^4$* |

[a] $\Delta V\% = \frac{(V_{opt}-V_{exp})}{V_{exp}} \cdot 100$

[b] Number in brackets are Ce site index for Ce sites in crystalline cells of given compounds.

[c] Superscript numbers refer to the multiplicity of bond length, when higher than 1.

The models were generated through classical molecular dynamics simulations by adopting the melt-quench method[55] implemented in the DL_POLY package.[56] Since the experimental densities of the investigated glasses have been published after the drawing up of the present manuscript the box side lengths were defined accordingly to density values calculated by the Priven empirical method,[57] which is encoded in the SciGlass package.[58] With this method the density ($d$) is computed by using the formula:

$$d = \sum_{i=1}^{N} g_i m_i n_i \sum_{i=1}^{N} m_i n_i \qquad (5)$$

Where $i$ is the index of the oxide, N is the number of oxides forming the glass, $m_i$ is the molar mass of the $i$-th oxide, $n_i$ is the number of atoms in the formula of the $i$-th oxide and $g_i$ is the partial coefficient of the $i$-th oxide..

**Table 4** Computed and experimental Ce-O bond distances and $Ce^{3+/4+}$ coordination numbers of the investigated glasses.

| Glasses | $Ce^{4+}$ % | <Ce-O> Å | | | | CN | | | |
|---|---|---|---|---|---|---|---|---|---|
| | exp[24] | exp<Ce-O> (± 0.01)[24] | MD<Ce-O> | MD<$Ce^{3+}$-O> | MD<$Ce^{4+}$-O> | exp CN (± 0.1)[24] | MD CN | MD CN $Ce^{3+}$ | MD CN $Ce^{4+}$ |
| CSP2 | 2 | 2.44 | 2.42 | 2.42(0.05) | n.d.[a] | 7.2 | 6.7 | 6.64 | n.d. |
| CSP3 | 3 | 2.43 | 2.41 | 2.41(0.02) | n.d. | 7.2 | 6.6 | 6.55 | n.d. |
| CSP4 | 1 | 2.43 | 2.41 | 2.41(0.01) | n.d. | 7.1 | 6.5 | 6.52 | n.d. |
| CSP6 | 3 | 2.41 | 2.42 | 2.42(0.02) | 2.28(0.01) | 6.9 | 6.6 | 6.56 | 7.48 |
| CSP9 | 3 | 2.40 | 2.42 | 2.42(0.05) | 2.28(0.00) | 6.8 | 6.6 | 6.56 | 7.66 |
| CSP[b] | --- | --- | 2.39 | 2.39(0.04) | 2.29(0.01) | --- | 6.6 | 6.50 | 7.78 |

[a] The value is not discussed because of the scant population of $Ce^{4+}$ in the composition.

[b] The experimental data for this composition is not available; for comparison purposes, the MD rigid ion model[19] yields: <$Ce^{3+}$–O> = 2.46 Å, <$Ce^{4+}$–O> = 2.24 Å, CN $Ce^{3+}$ = 6.7, CN $Ce^{4+}$ = 6.5

The parameters $g_i$ were derived by using experimental data on numerous properties of 222590 glasses and glass forming melts. This method can be applied to compute densities for glasses and glass forming melts belonging to various oxide systems: it was shown that the standard deviation lies around 4% when 64 oxides are included.[59]

Glass structural models were heated and held at 3200 K for 100 ps in the NVT ensemble ensuring a suitable melting of the samples. The liquids were subsequently cooled to 300 K at a nominal cooling rate of -5 K/ps and the resulting glass structures subjected to a final NVT trajectory of 0.3 ns. Because of the employment of non-experimental densities, the final glass models were relaxed for 0.2 ns, at 300K and atmospheric pressure using the Berendsen NPT ensemble. The final densities presented deviations less than 4.5% with respect to the Priven values. Table S1 of the ESI compares the experimental density ($\rho_{exp}$) with those computed with the PRIVEN method ($\rho_{PRIVEN}$ ) and after NPT MD simulations at 300K ($\rho_{NPT}$).

The densities of the CSP glasses investigated in this work are very close to the experimental ones (errors less than 5.7%) and thus we are quite confident of the validity of our structural models.

The integration of the equation of motion was performed by the leap-frog algorithm with a timestep of 0.2 fs, a value which is small enough to account for the high frequency vibrations of the core-shell system.[55] The presented method was successfully applied to generate good structural models for silicate,[28, 60] phosphosilicate[38, 61] and aluminosilicate[36, 37, 62] glasses. t

The structural analysis of the models was performed on the NPT relaxed structures by a homemade code[55] on 2001 configurations sampled at regular intervals during 0.2 ns of an NVT MD trajectory at 300K. The cutoff values for the analysis of the first coordination shells were fixed to 2.0 Å for Si-$O_s$, 2.0 Å for P-$O_s$, 3.0 Å for Al-$O_s$, 3.0 Å for $Ce^{3+}$-$O_s$ and 2.8 Å for $Ce^{4+}$-$O_s$. These values were obtained from the first minimum of the corresponding partial distribution function, which will be presented and discussed later for Ce atoms.

## Results and discussion

### Validation of the Buckingham parameters for $Ce^{3+}$-O and $Ce^{4+}$-O pairs.

To test the reliability of the new parameters the final force field has been used to carry out a relaxed geometry optimization of 7 crystalline reference phases. The structural variations before and after the optimization have been monitored, and the results obtained for cell parameters, unit cell volume, and Ce-O bond lengths are listed in Table 3, together with the experimental counterparts. The data values obtained in this study by means of the rigid ionic potential parameters proposed by Du et al.[19] (also listed in Table 3) allow a direct comparison of the performance of the two potential models on the local environment around Ce ions.

Cell parameters generally vary within 0.1 Å, with a maximum variation of 0.5 Å (2.0% of experimental value) for the *c* parameter of the $Ce_4(Si_2O_7)_2$ crystal, that also presents the most severe, but still modest, volume variation of +3.6% (+5.3% with the RI model). It is worth noticing that the CS model provides cell parameter variations for $Ce_2O_3$ and $CeO_2$ between 0.06% and 0.08%, whereas the RI potentials yields a deviation between 0.2% and 0.3% on the unit cell parameters and of 0.6% and 2.9% on cell volumes, as reported in Table 3.

The variation in the average Ce-O distance per Ce site (<Ce-O>) is within 0.02 Å, which is similar to what Du et al. obtained with the RI potential.[19] The CS model provides a maximum variation in <Ce-O> bond distances of -0.05 Å for one of the two Ce sites in $CeP_5O_{14}$ crystal, whereas the RI model yields a maximum deviation of 0.06 Å for the $CePO_4$ crystal phase. The variation in the length of single Ce-O bonds is generally within 0.05 Å, and shows a maximum of +0.2 Å (+0.4 Å with the RI model) only for the longer Ce-O distance in Ce sites of the $Ce_4(Si_2O_7)_2$ crystal.

In summary, these results demonstrate that the proposed force field is able to reproduce the Ce environment in crystals with high accuracy.

### Ce local environment in glasses.

Table 4 reports the comparison between the computed and experimental Ce-O bond distances (<Ce-O>), and Ce coordination numbers (CN), together with experimental amount of $Ce^{4+}$ (given as percentage respect to total Ce) in the investigated glasses. The exhaustive Ce K-edge EXAFS work of Rygel et al.[24] is the experimental reference for Ce local environment in CSP glasses.

It is worth noticing that <Ce-O> is the only direct, accurate experimental observable, exp<Ce-O>, while experimental CN, expCN, has been calculated by linear interpolation of exp<Ce-O> data[24] and bear major uncertainty. The exp<Ce-O> values decrease with the $Ce_2O_3$ content from 2.44 Å, for CSP2, to 2.40 Å, for CSP9, whereas the MD<Ce-O> remains almost constant on 2.41-2.42 Å.

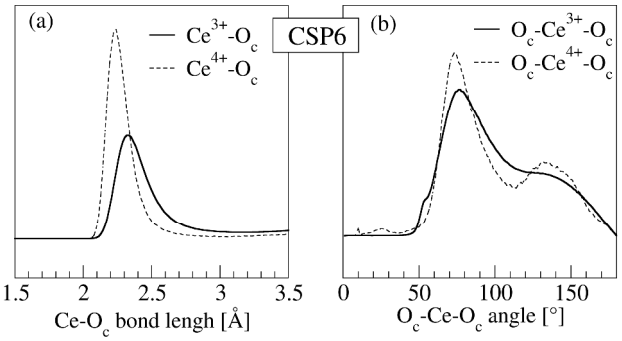


**Fig. 1** a) Partial distribution functions of Ce-$O_c$ atom pairs and b) $O_c$-Ce-$O_c$ bond angle distributions of the CSP6 glass.

However, the difference between the two counterparts never exceeds 0.02 Å, which indicates that the proposed force field very well reproduces this structural feature. As for the coordination numbers, MD simulations results reveal that Cerium ions are surrounded by 6.5-6.7 non-bridging oxygens (NBOs). These values are slightly smaller than those given by Rygel et al.[24] which are in the range 6.9 ÷ 7.2 (± 0.1), but agree very well with the X-ray diffraction measurements performed by Cole et al.[20], who determined a CN value of about 6.5 units in Ce-phosphate glasses. By comparing MD simulations, diffraction and EXAFS measurements with predictions based on the bond valence, Mountjoy[63] also found that the Rare Earth CN in $(RE_2O_3)_x(P_2O_5)_{1-x}$ glasses varies between 6.5 and 7.0 when $0.18 \leq x \leq 0.28$.

Figure 1a shows the partial distribution functions (PDFs) of $Ce^{3+}$-$O_c$ and $Ce^{4+}$-$O_c$ pairs of the CSP6 glass. The $Ce^{3+}$-$O_c$ PDFs are less symmetric and wider than the $Ce^{4+}$-$O_c$ ones, and the $Ce^{3+}$-$O_c$ bond length is generally longer. Thus, the higher field strength of the $Ce^{4+}$ ion yields more ordered short and medium environments than $Ce^{3+}$.

The analysis of the average bond distances between $Ce^{3+}$ and $Ce^{4+}$ cations and $O_c$, reveals that the $^{MD}$<$Ce^{3+}$-$O_c$> lies between 2.41 and 2.42 Å, while the $^{MD}$<$Ce^{4+}$-$O_c$> was found to be 2.28 Å for both CSP6 and CSP9 glasses. The $^{MD}Ce^{3+}$-O and $^{MD}Ce^{4+}$-O interatomic distances found in the present study are in line with the <Ce-O> distances found in the crystalline samples reported in Table 3 (*italic* fonts). Crystalline phases containing $Ce^{3+}$ exhibit a <Ce-O> between 2.34 Å and 2.72 Å, while $Ce^{4+}$-containing crystals show the <Ce-O> varying between 2.27 Å and 2.36 Å.

A good agreement is also found between our $^{MD}$<$Ce^{4+}$-$O_c$> distances and those reported by Du et al.[19], which ranges between 2.24-2.28 Å. Instead, our $^{MD}$<$Ce^{3+}$-$O_c$> bond lengths are 0.04-0.05 Å smaller than those found by Du et al.[19] in silicophosphate glasses.

Both $Ce^{3+}$ and $Ce^{4+}$ atoms are coordinated by NBOs only. The results reported in Table 4 show that $Ce^{4+}$ average CN is 7.5 and 7.7 for CSP6 and CSP9, respectively. The CN of $Ce^{4+}$ value is about 1 unit higher than average $Ce^{3+}$ CN, which is almost constant to 6.5-6.7. These results are in partial disagreement with those obtained by Du et al.[19] in their computational work. In fact, they found that the CN of $Ce^{4+}$ is slightly lower (6.5) than that of $Ce^{3+}$ (6.7). Instead, our results are in line with those found in crystals where $Ce^{3+}$ mainly presents a CN value of 7 units, while $Ce^{4+}$ CN is 8.

Although shorter bond lengths are usually associated to smaller CN, the case of $Ce^{4+}$ can be explained by its very high field strength that allows a more effective packing of O ions.

The comparison of Bond Angle Distributions (BADs) (Fig. 1b) of $O_c$-$Ce^{3+}$-$O_c$ and $O_c$-$Ce^{4+}$-$O_c$ confirms that $Ce^{3+}$ coordination environment is more disordered than the $Ce^{4+}$ one.[19] Both $O_c$-$Ce^{4+/3+}$-$O_c$ BADs present two peaks at 70-80° and 140°, however those of the $O_c$-$Ce^{4+}$-$O_c$ BADs are narrower. The differences highlighted by the BADs are confirmed by the fact that the CN distributions for $Ce^{3+}$ is wider than for $Ce^{4+}$ (Figure 2; Table S2 of the Electronic Supporting Information (ESI)).

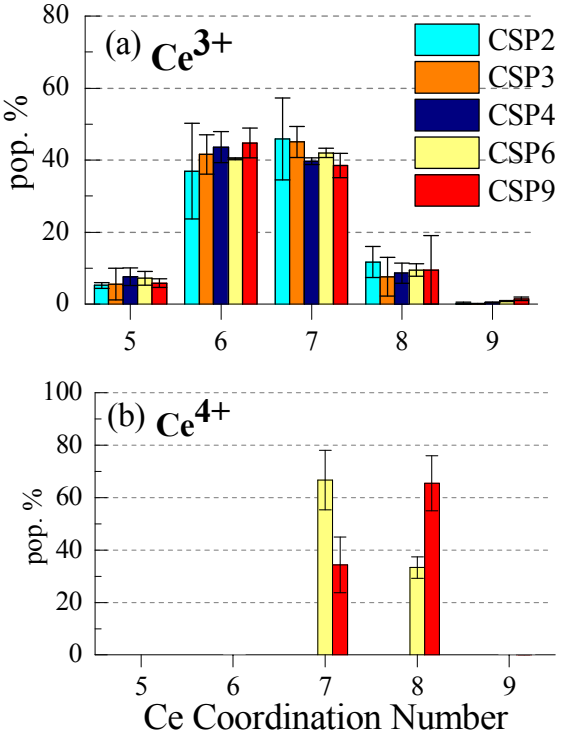


**Fig. 2** Coordination Number (CN) distributions for (a) $Ce^{3+}$ in CSP2, CSP3, CSP4, CSP6 and CSP9 glasses and (b) $Ce^{4+}$ in CSP6 and CSP9 glasses.

**Short-range order of Si, P and Al**

The average CN (<MDCN>) of P, Si and Al cations, their CN distributions and their average bond distances with Oc, MD<T-Oc> are reported in Table 5.

As expected, due to their network former roles, both P and Si generally exhibit a CN around 4. In particular, the CN of P is 4.00-4.01 in all models, whereas the CN of Si ranges from 4.02 to 4.04 in the CSP2, CSP3, CSP4 and CSP6 compositions. This is due to the presence of a maximum of 5.1% of 5-folded Si. The obtained data agree with experimental findings of highly coordinated Si in silicophosphate glasses with $P_2O_5$ > 30%.[64, 65] Among 5-coordinated Si, some Si($Q^5$) sites, i.e.: Si coordinated by 5 BOs, are present. They amount to 4.5%, 2.2%, 2.2%, 3.4% and 0.0% of total Si in CSP2, CSP3, CSP4, CSP6 and CSP9, respectively.

Cite this: DOI: 10.1039/c0xx00000x

www.rsc.org/xxxxxx

# ARTICLE TYPE

**Table 5** $^{MD}$<T-$O_c$>, $^{MD}$<T-BO>, $^{MD}$<T-NBO> bond lengths and CNs of T=Si/P/Al cations in the investigated glasses. Data for Si in CSP9 are omitted because of its negligible presence in the composition (0.7 mol%). The standard deviations are reported in parenthesis.

| Glasss | $^{MD}$<T-$O_c$> [Å] | $^{MD}$<T-BO> [Å] | $^{MD}$<T-NBO> [Å] | $^{MD}$<CN> | CN 3 | 4 | 5 | 6 |
|---|---|---|---|---|---|---|---|---|
| | | | | P | | | | |
| CSP2 | 1.55 (0.01) | 1.58 (0.01) | 1.49 (0.01) | 4.01 | 0.2 (0.1) | 99.0 (0.5) | 0.8 (0.5) | 0.0 |
| CSP3 | 1.55 (0.01) | 1.58 (0.01) | 1.49 (0.01) | 4.01 | 0.1 (0.1) | 99.3 (0.2) | 0.6 (0.2) | 0.0 |
| CSP4 | 1.55 (0.01) | 1.59 (0.01) | 1.49 (0.01) | 4.00 | 0.1 (0.1) | 99.3 (0.3) | 0.6 (0.3) | 0.0 |
| CSP6 | 1.56 (0.01) | 1.61 (0.01) | 1.50 (0.01) | 4.00 | 0.1 (0.1) | 99.3 (0.2) | 0.6 (0.2) | 0.0 |
| CSP9 | 1.56 (0.01) | 1.63 (0.01) | 1.51 (0.01) | 4.01 | 0.1 (0.2) | 98.6 (2.0) | 1.3 (0.9) | 0.0 |
| CSP | 1.55 (0.01) | 1.60 (0.01) | 1.50 (0.01) | 3.99 | 0.9 (0.1) | 99.1(1.0) | 0.0 (0.0) | 0.0 |
| | | | | Si | | | | |
| CSP2 | 1.63 (0.01) | 1.63 (0.01) | 1.56 (0.01) | 4.02 | 0.0 | 94.2 (2.4) | 5.1 (2.9) | 0.0 |
| CSP3 | 1.63 (0.01) | 1.63 (0.01) | 1.56 (0.01) | 4.04 | 0.1 (0.1) | 95.7 (0.7) | 4.2 (0.7) | 0.0 |
| CSP4 | 1.63 (0.01) | 1.63 (0.01) | 1.56 (0.01) | 4.04 | 0.0 | 95.9 (0.3) | 4.1 (0.3) | 0.0 |
| CSP6 | 1.63 (0.01) | 1.63 (0.01) | 1.55 (0.00) | 4.04 | 0.0 | 96.0 (2.2) | 4.0 (2.4) | 0.0 |
| CSP | 1.63 (0.01) | 1.63 (0.01) | 1.55 (0.01) | 4.04 | 0.0 | 96.0 (1.3) | 4.0 (2.0) | 0.0 |
| | | | | Al | | | | |
| CSP2 | 1.83 (0.01) | --- | --- | 5.04 | 0.5 (0.1) | 16.0 (7.1) | 62.3 (3.6) | 21.3 (8.6) |
| CSP3 | 1.84 (0.01) | --- | --- | 5.08 | 0.0 | 11.4 (2.5) | 68.1 (4.5) | 19.4 (0.2) |
| CSP4 | 1.84 (0.01) | --- | --- | 5.22 | 0.0 | 8.9 (1.8) | 61.8 (1.6) | 29.5 (3.6) |
| CSP6 | 1.84 (0.01) | --- | --- | 5.09 | 0.4 (0.4) | 8.4 (4.7) | 72.1 (7.9) | 19.2 (4.0) |
| CSP9 | 1.84 (0.01) | --- | --- | 5.30 | 0.0 | 2.6 (1.7) | 65.0 (3.6) | 32.5 (5.0) |

In all models, the <P-$O_c$> bond lengths are about 1.55 Å, while the <Si-$O_c$> are about 1.61 Å, again in very good agreement with experimental findings on aluminosilicates,[66] silicophosphate[67] and aluminophosphate[68] glasses. Table 5 also reports the computational analysis of Si and P bond distance with respect to bridging (BO) and non-bridging (NBO) oxygens speciation.

In all compositions, <P-BO> and <P-NBO> measure ~1.59-1.62 Å and ~1.49 Å, respectively, showing a very good agreement with the experimental counterparts (1.60 Å and 1.50 Å)[68]. Interestingly, the <P-BO> bond length increases with the $P_2O_5$ content and, thus, with the amount of P-BO-P bridges, while the <P-NBO> distance remains constant to 1.49-1.50 Å. The <Si-BO> is ~1.63 Å, i.e. within the range of 1.61-1.64 Å found for the Si-BO in silicate glasses by experimental studies, depending on the content of modifier cations in the glass.[69,70] The <Si-NBO> measures ~1.55 Å and is 0.08 Å shorter than <Si-BO>, according to experimental findings on several crystal phases, where Si-BO and Si-NBO bond length differ of 0.06-0.08 Å.[71]

Aluminum average coordination number (Table 5) ranges between 5.04 and 5.30, and the CN distribution varies from 4 to 6 in all glasses. The most populated sites are 5-fold (~60-70%) and 6-fold Al (~20-30%), while Al in tetrahedral coordination represent about the 10% of total Al atoms. The Al CN distribution and the average Al CN found in this work are coherent with the role of network modifier highlighted by NMR experiments for low concentration of $Al_2O_3$ in RE containing glasses[72, 73]. Finally, the $^{MD}$<Al-$O_c$> bond length is ~1.8 Å in good agreement with the experimental results of highly-coordinated Al in Ce-containing aluminophosphate glasses.[68]

### Medium-range order of Si, P and Al

The medium-range environment of P and Si is described by the $Q^n$ species distribution and the characterization of the second coordination sphere of former cations, which provide an overview on network polymerization level and network chemical disorder, respectively. The results are collected in Tables S3 and S4 available in ESI.

The $Q^n$ distribution of tetrahedral P, P($Q^n$), (Figure 3a) is dominated by $Q^2$ and $Q^3$ species with small amounts of $Q^1$ species for CSP2, CSP3 and CSP4 glasses, whereas the $Q^2$ species are prevalent in the CSP6 and CSP9 glasses, where smaller amounts of $Q^1$ and $Q^3$ species are also found.

Figure 3b shows that the $Q^n$ distribution of silicon is always dominated by $Q^4$ species (~90% of total Si) with a small amount of $Q^3$ species (~5%). These distributions reveals that Si atoms form the most polymerized part of the network, and the phosphate network depolymerizes with the addition of $Ce_2O_3$ and $P_2O_5$. Ring size analysis, reported in Figure S1 in ESI, confirms this trend. Our results are in agreement with NMR experiments, which have revealed that the addition of small amount of $P_2O_5$ to binary alkali-silicate glasses leads to more polymerized silica networks (since phosphorous attracts modifier cations, thus forming metaphosphate groups),

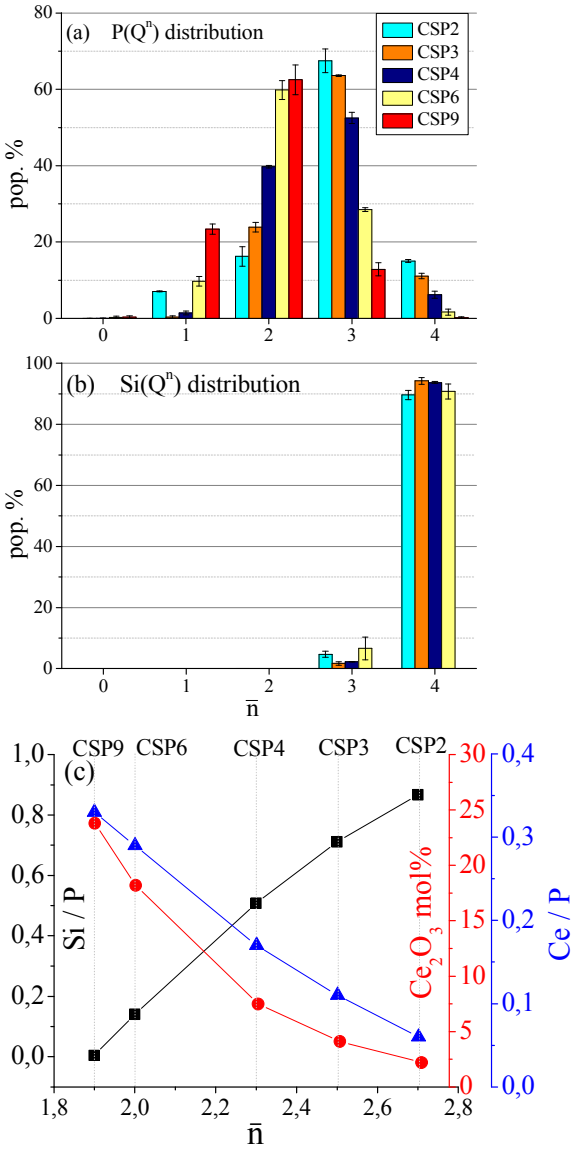


**Fig. 3**. Medium-range order of P and Si cations. (a) P($Q^n$) distribution for all compositions; (b) Si($Q^n$) distribution for all compositions with exception of the CSP9 glass (too small amount of Si in the models); (c) average number of BOs bonded to P atoms as a function of Si/P (black), $Ce_2O_3$ content mol % (red) and Ce/P (blue).

whereas highly coordinated Si species appears at high phosphorous concentration.[64, 74, 75]

The relation between the average number $n$ of BOs bonded to P atoms, $\bar{n}$, the $Ce_2O_3$ content and the Si/P and Ce/P ratio is shown in Figure 3c (the numerical values are reported Table S4 of the ESI).

The figure shows that $\bar{n}$ monotonically decreases with the $Ce_2O_3$ content and with the Ce/P ratio, while it increases with the Si/P ratio. This implies that Ce-containing silicophosphate glasses with a specific value of $\bar{n}$ (and thus with a specific degree of polymerization) can be designed by varying the Ce/P and Si/P ratios.

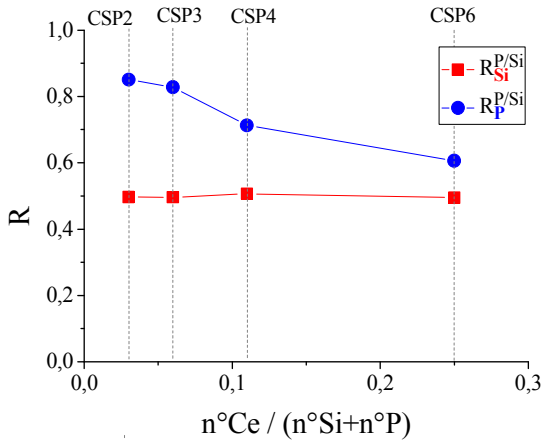


**Fig. 4**. Network chemical disorder investigated by plotting the ratio $R_T^{P/Si}$ (T=Si and P) vs the variation of the ratio n°Ce/(n°P+n°Si) for CSP2, CSP3, CSP4 and CSP6 glasses. Discussion on CSP9 omitted because of the negligible amount of Si atoms in the models.

Moreover, an overview of P-Si intermixing in each composition is given by the coordination numbers of each former ion (T) with respect to the number of Si and P ions in their second coordination sphere ($CN_T^{Si}$ and $CN_T^{P}$). The network chemical disorder is quantified by the factor $R_T^{P/Si}$ for both Si (Eq. 6) and P (Eq. 7). This factor is given by the ratio of $CN_T^{P}$ and $CN_T^{Si}$, normalized with respect to the ratio of number of P and Si in the models (Table 2).

$$R_{Si}^{P/Si} = (CN_{Si}^{P}/CN_{Si}^{Si})/(n°P/n°Si) \quad (6)$$

$$R_{P}^{P/Si} = (CN_{P}^{P}/CN_{P}^{Si})/(n°P/n°Si) \quad (7)$$

If $R_T^{P/Si}$ is equal to 1, then T is equally surrounded by P and Si; if $R_T^{P/Si} < 1$, then T is preferentially surrounded by Si; and if $R_T^{P/Si} > 1$, T is preferentially surrounded by P.

Figure 4 shows the plot of $R_{Si}^{P/Si}$ (squares) and $R_P^{P/Si}$ (circles) versus the ratio n°Ce/(n°Si+n°P) that characterizes each composition. Both the $R_{Si}^{P/Si}$ and $R_P^{P/Si}$ values (reported in Table S5) are smaller than 1, meaning that both the P and Si environments are richer in Si rather than in P. However, while $R_P^{P/Si}$ value is constant around 0.5 for all compositions, $R_{Si}^{P/Si}$ decreases from 0.86, in CSP2, to 0.60, in CSP6, indicating that Si environment becomes richer in Si tetrahedra by increasing the Ce content. These trends, together with those reported for the $Q^n$ distribution of P in Figure 3a**,** indicate that the increment of Ce content leads to the formation of polymerized silica-rich and Ce-phosphate regions. Therefore, as also observed by Du et al.,[19] phosphate groups tend to act as solvation shells for Cerium ions. An overview of the structural differences for CSP3 and CSP6 compositions is shown in Figure 5. In CSP3 glass (Fig. 5a) P and Si are mixed in polymerized regions, while CSP6 (Fig. 5b) clearly lacks of Si-P intermixing.

It is worth stressing that, although our results are in qualitative agreement with those reported by Du et al.[19] with

Cite this: DOI: 10.1039/c0xx00000x

www.rsc.org/xxxxxx

# ARTICLE TYPE

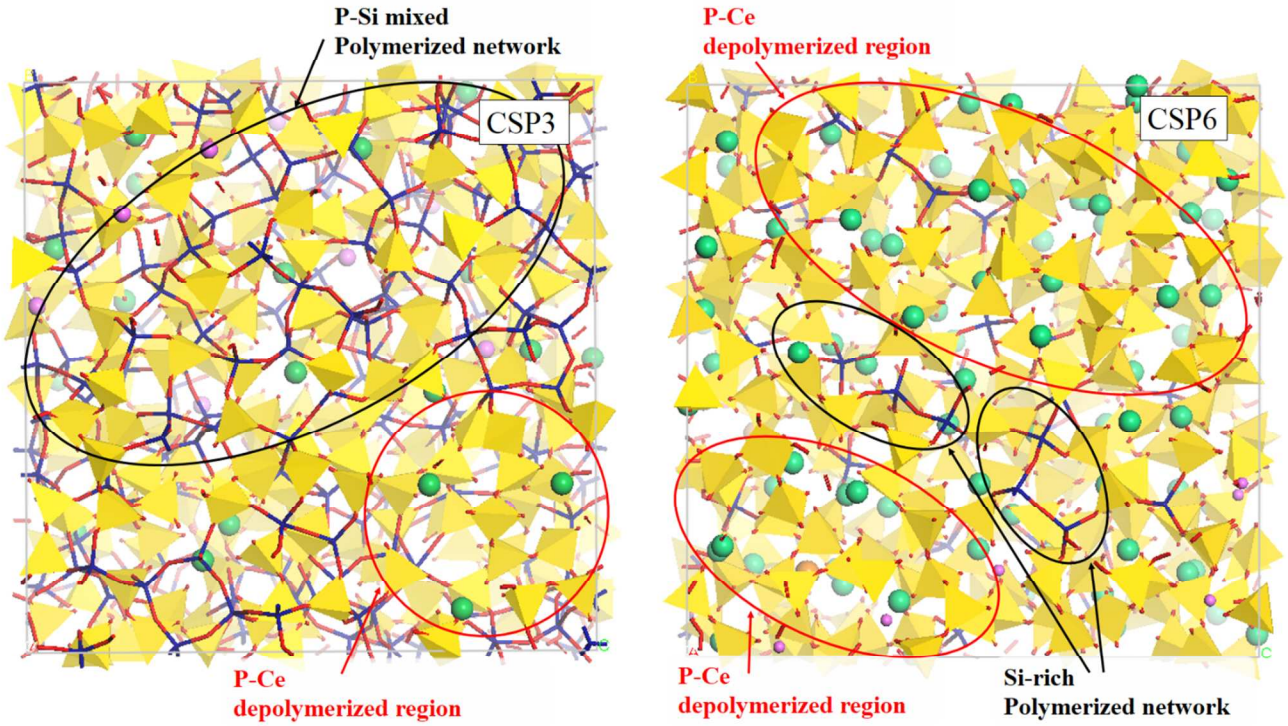


**Fig. 5** Change in network structure moving from CSP3 (left) to CSP6 (right) composition. Yellow polyhedra are P units, dark blue sticks represent Si, red sticks are O, violet spheres are Al, green spheres are $Ce^{3+}$ and orange spheres are $Ce^{4+}$

respect to the solvation role played by the phosphorous ions, a quantitative agreement is lacking. In fact, the $Q^n$ distributions of structural models derived in this study by means of the CS and the RI models on the CSP glass composition previously investigated by Du et al.[19] (Table 2) are quite different. The RI model provides a broader $Q^n$ distribution for phosphorous, constituted by 2.9%, 29.9%, 49.8% and 16.5% of $Q^1$, $Q^2$, $Q^3$ and $Q^4$ species, respectively; while the CS model yields a narrower distribution dominated by $Q^2$ (50.7%) and $Q^3$ (35.7%) species, with a negligible amount of $Q^4$ species (table S6 of the ESI).

To confirm the accuracy of the CS model in reproducing the medium-range environment of the P ions the $Q^n$ and the P-O-P bond angle distributions have been computed for a CaO-$P_2O_5$ glass, for which experimental data are available.[76, 77] The results obtained by means of the RI and CS models are reported in Table S7 and Figure S2 of the ESI. Once again, our results demonstrate the superiority of the CS model to reproduce the medium range order of oxide glasses. This superiority is due to the explicit account of the polarization of O atoms. In fact, Tilocca[27] recently showed that the shell model well reproduces the dynamical evolution of the interconversion between $Q^n$ species during the cooling of the melt as it happens in Car-Parrinello MD simulations. This aspect is very important because the different $Q^n$ distributions leads to different chemical disorder (see Table S8 of the ESI) and different Ce clustering. As physical properties of glasses, i.e.: bioactivity, chemical durability, optical properties, etc…, strongly depend on their medium-range order, a modelling protocol able to reproduce them correctly is necessary when the final aim is to predict glass behavior as a function of the composition.

The Aluminium second coordination sphere was studied within a cutoff of 5.00 Å, with respect to all cations, ${}^{MD}CN^{M}_{Al}$ (M is Si, P, $Ce^{3+}$or $Ce^{4+}$). We compared ${}^{MD}CN^{M}_{Al}$ to coordination numbers calculated accordingly to random distributions of cations inside the box, ${}^{random}CN^{M}_{Al}$ (Equation 8).

$$ {}^{random}CN^{M}_{Al} = \frac{4}{3}\pi \cdot r_{cut-off}{}^{3} \cdot \frac{n_M}{V_{box}} \qquad (8) $$

where $n_M$ and $V_{box}$ are reported in Table 2. The ${}^{MD}CN^{M}_{Al}$ data values listed in Table 6 highlight how, moving from CSP2 to CSP9, Al surroundings become richer in $Ce^{3+}$ and P, and poorer in Si. The comparison between random and MD-derived coordination numbers shows that, for every composition, the ${}^{random}CN^{M}_{Al}$ are higher than the ${}^{MD}CN^{M}_{Al}$ for $Ce^{3+}$ and Si, and smaller for P. Therefore, Al is preferably allocated in phosphate-like glass regions and tends to avoid mixing with Ce ions and silica-like network regions.

Cite this: DOI: 10.1039/c0xx00000x

www.rsc.org/xxxxxx

# ARTICLE TYPE

**Table 6** Coordination number of Al with respect to other cations (M), $CN_{Al}^{M}$, within a cutoff of 5.00 Å. MD-derived ($CN_{Al,MD}^{M}$) data are compared to data calculated accordingly to random distributions ($CN_{Al,random}^{M}$).

| | CSP2 | CSP3 | CSP4 | CSP6 | CSP9 |
|---|---|---|---|---|---|
| $CN_{Al,MD}^{Si}$ | 3.6 (0.5) | 3.4 (0.5) | 3.0 (0.5) | 1.0 (0.1) | 0.0 (0.0) |
| $CN_{Al,random}^{Si}$ | 5.4 | 4.6 | 3.6 | 1.1 | 0.0 |
| $CN_{Al,MD}^{P}$ | 7.4 (0.3) | 7.1 (0.3) | 7.9 (0.2) | 9.2 (0.5) | 9.1 (0.5) |
| $CN_{Al,random}^{P}$ | 6.1 | 6.5 | 7.0 | 8.1 | 8.5 |
| $CN_{Al,MD}^{Ce3+}$ | 0.1 (0.1) | 0.2 (0.1) | 0.5 (0.2) | 1.0 (0.1) | 1.3 (0.2) |
| $CN_{Al,random}^{Ce3+}$ | 0.4 | 0.7 | 1.2 | 2.3 | 2.6 |

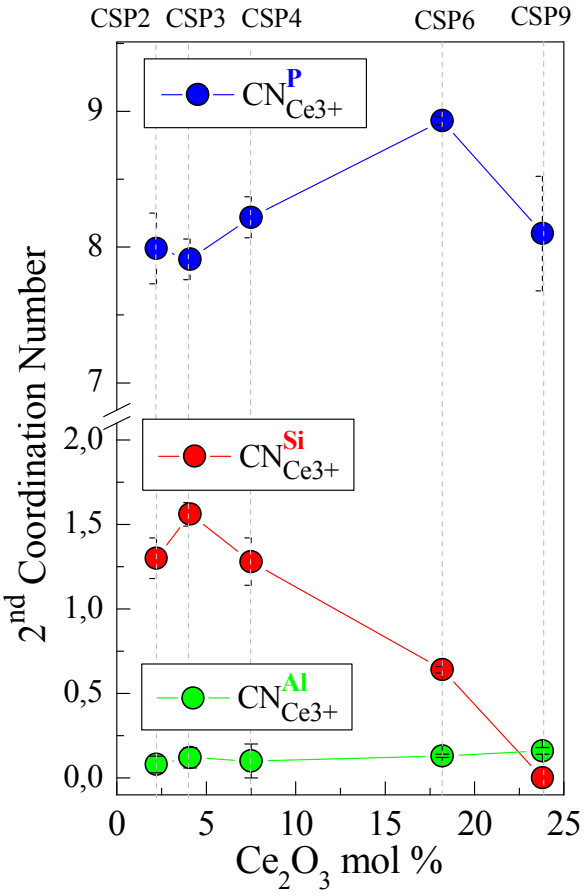


**Figure 6**. Analysis of $Ce^{3+}$ second neighbors within a cutoff of 5.00 Å. Coordination numbers with respect to P (blue), Si (red) and Al (green) in Ce second coordination sphere.

**Ce second coordination shell and clustering.**

The coordination numbers of $Ce^{3+}$ with respect to P, ($CN_{Ce}^{P}$), Si, ($CN_{Ce}^{Si}$), and Al, ($CN_{Ce}^{Al}$), are reported in Figure 6 and in Table S9 of the ESI. As expected from the previous discussion, the $Ce^{3+}$ environment becomes richer in P and poorer in Si moving from CSP2 to CSP9. The variation of $CN_{Ce}^{P}$ and $CN_{Ce}^{Si}$ with the composition is gradual, from 7.99 to 8.71, and from 1.30 to 0.00, respectively.

Since Ce-Ce clustering is known to affect the optical properties of glasses and is related to the Ce solubility, we characterized Ce clustering by seeking the formation of Ce-O-Ce linkages and counting the size of clusters within a Ce-Ce cutoff of 5.0 Å

Figure 7a shows the cluster size distributions for the investigated glasses. In all glasses, the distribution is dominated by isolated $Ce^{3+}$ and $Ce^{4+}$ ions, supporting the findings that these ions are well solvated by $PO_4$ tetrahedra in the glasses. However, at the CSP6 composition ($Ce_2O_3$ = 18.2 mol%), a rapid decrement of isolated Ce ions and a substantial increment of the population of clusters with larger sizes is observed. This shows that Ce clustering begins at the CSP6 composition. These results are in agreement with those reported by Rygel et al.[24] who estimated that Ce clustering should be present in composition where $Ce_2O_3$ > 15 mol%. This estimation was done by comparing the Ce coordination number, $^{Ce}CN$, with the amount of terminal oxygens (TO comprises NBOs and oxygens bearing the double P=O bond) per Ce atoms, TO/Ce, calculated accordingly to a segregation model.[24] Clustering is expected for $^{Ce}CN$ > TO/Ce, because in this condition the Ce atoms must share some of the TOs provided by phosphate network, and Ce-O-Ce bridges appear.

In Table 4 we have compared the TO/Ce ratio provided by our MD-derived models to the Ce coordination number. In agreement with the results obtained by Rygel et al.[24], we found that the CN of Ce ions becomes higher than TO/Ce ratio between the CSP4 and the CSP6 composition. Figure 7b reports the plot of the Ce CN and TO/Ce ratio versus the Ce/P ratio that characterizes each composition.

Figure 7b also shows that the average cluster size (and thus the average degree of clustering) increases with the Ce/P ratio of the glasses in a monotonic way: 1.05, 1.09, 1.26, 1.92 and 1.99 for CSP2, CSP3, CSP4, CSP6 and CSP9, respectively. This further analysis confirms that Ce clustering occurs in CSP6 and CSP9 compositions.

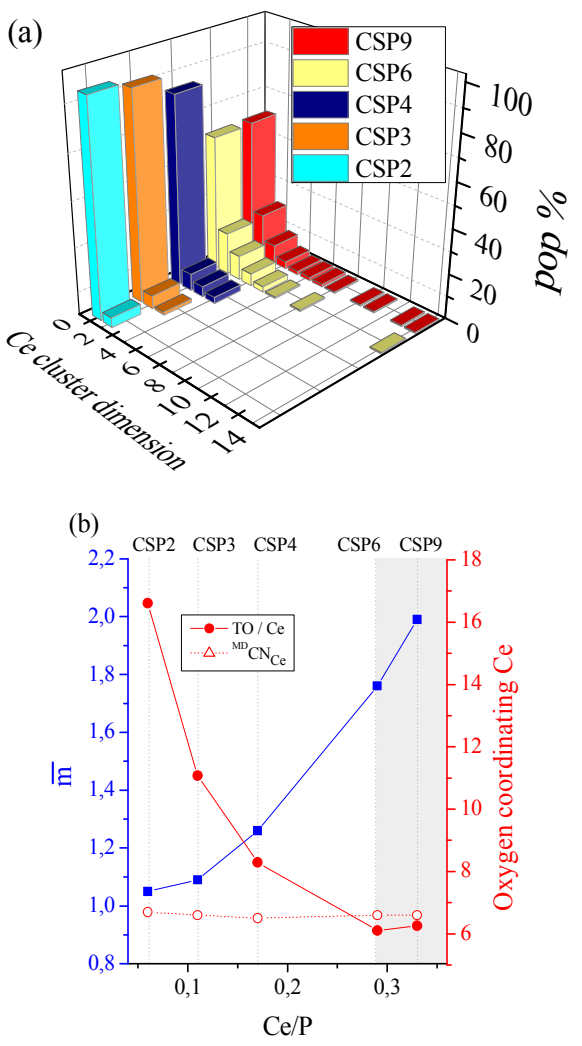


**Fig. 7** (a) Ce-Ce cluster size distributions in CSP2, CSP3, CSP4, CSP6 and CSP9 glasses. (b) The full square symbols represent the average cluster size as a function of the Ce/P ratio in the glasses; the full circles represent the TO bonded to P and available for Ce coordination as a function of the Ce/P ratio whereas the empty circles represent the Ce coordination numbers as a function of the Ce/P ratio.

## Conclusions

In this work, we have presented a core-shell force field for Ce-containing glasses compatible with the potential forms and parameters present in the literature for silicophosphate glasses. The force field has been parametrized on 5 crystalline phases containing $Ce^{3+}$ ($Ce_2O_3$, $CeP_5O_{14}$, $Ce_2Si_2O_7$, $CePO_4$ and Ce-florencite ($Al_3CeP_2O_{14}H_6$)) and on 2 crystalline phases containing $Ce^{4+}$ ($CeO_2$ and $CeSiO_4$).

The proposed force field reproduces accurately the $Ce^{3+}$ and $Ce^{4+}$ short range environment in both crystalline and amorphous structures. Moreover, the force-field has been used to investigate the structure of five silicophosphate glasses containing an increasing amount of Ce and P and a decreasing amount of Si.

The $Ce^{3+}$ and $Ce^{4+}$ short-range environments are found to be very different: the $Ce^{3+}$ coordination number (~6.5) is about 1 unit smaller than the $Ce^{4+}$ one (~7.5), and the $Ce^{3+}$ environment is more disordered, mimicking the structural arrangement of $Ce^{3+}$ and $Ce^{4+}$ in several crystalline phases.

The analysis of medium-range order of all cations present in the models has allowed us to depict a precise picture of the structure of the glasses under study. The investigation of $Q^n$ speciation of P and Si and of the network chemical disorder have suggested that polymerized silica-like regions and depolymerized phosphate-like regions are formed. P tetrahedra act as Ce "solvation" shell, as observed in previous works.[14, 19, 24] The increase of $Ce_2O_3$ content in the glass enhances the Si and P separation, attracting P polyhedra towards Ce-containing depolymerized regions.

Beyond the well-known correlation between the high amount of $P_2O_5$ and the small Ce clustering occurrence, we found that Ce clustering in silicophosphate glasses begins for Ce/P ratios between 0.17 and 0.29.

These findings might have important implications also for other glass compositions. For example, in bioactive glasses the addition of Ce ions (which enhances the antioxidant properties of glasses) could compromise the formation of the hydroxyapatite layer on their surfaces because of the appearance of insoluble Ce-rich phases that increase chemical durability.

## Acknowledgments

The authors thank Dr. Gianluca Malavasi and Prof. Maria Cristina Menziani for the fruitful discussions. Our acknowledgements also go to the computational resources technician, Maria Cristina Murari. This work was supported by a grant from the University of Modena and Reggio Emilia entitled 'The role of Cerium oxidation state in bioactive glasses used as biomaterials of 3rd generation'.

## Notes and references

[a] *Dipartimento di Scienze Chimiche e Geologiche, Università degli Studi di Modena e Reggio Emilia, via G. Campi 183, 41125, Modena, Italy. E-mail:elisa.gambuzzi@unimore.it; alfonso.pedone@unimore.it*

† Electronic Supplementary Information (ESI) available: tables containing numerical data used to build Figures 2, 4, 6 and 7 and figures showing the ring size distribution and the P-O-P BADs of the $CaO$-$P_2O_5$ glass. See DOI: 10.1039/b000000x/

1 O. Gorodetskaya, R. Reisfeld and C. K. Jorgensen, *Bol. Soc. Esp. Ceram. Vid.*, 1992, **31-c**, 479.
2 R. J. Ginther, *Trans. Nucl. Sci*, 1960, **7**, 28.
3 J. S. Stroud, *J. Chem. Phys.*, 1961, **35**, 844.
4 J. S. Stroud, *J. Chem. Phys.*, 1962, **37**, 836.
5 J. S. Stroud, *J. Chem. Phys.*, 1965, **43**, 2442.
6 C. Leonelli, G. Lusvardi, G. Malavasi, L. Menabue and M. Tonelli, *J. Non-Cryst. Solids*, 2003, **316**, 198.
7 H. Iwanaga, *Materials*, 2010, **3**, 4080.
8 L.-L. Lee and D.-H. Tsai, *J. Mater. Sci. Lett.*, 1994, **13**, 615.
9 S. Sen, *J. Non-Cryst. Solids*, 2000, **261**, 226.
10 J. Du and A. N. Cormack, *J. Non-Cryst. Solids*, 2005, **351**, 2263.
11 E. M. Larson, A. J. G. Ellison, F. W. Lytle, A. Navrotsky, R. B. Greegor and J. Wong, *J. Non-Cryst. Solids* 1991, **130**, 260.
12 T. Shaller, J. F. Stebbins and M. C. Wilding, *J. Non-Cryst. Solids*, 1999, **243**, 146.
13 S. Prabakar, K. J. Rao and C. N. R. Rao, *J. Mater. Res*, 1991, **6**, 592.
14 K. Arai, H. Namikawa, K. Kumata and T. Honda, *J. Appl. Phys.*, 1985, **59**, 3460.

15 J. E. Shelby and J. T. Kohli, *J. Am. Chem. Soc.*, 1990, **73**, 61.
16 S.-L. Lin and C.-L. Hwang, *J. Non-Cryst. Solids*, 1996, **2002**, 61.
17 D. Ilieva, B. Jivov, D. Kovacheva, T. Tsacheva, Y. Dimitriev, G. Bogachev and C. Petkov, *J. Non-Cryst. Solids*, 2001, **293-295**, 562.
18 N. E. Rashid, B. L. Phillips and S. H. Risbud, *J. Mater. Res.*, 2000, **15**, 2463.
19 J. Du, L. Kokou, J. L. Rygel, Y. Chen, C. G. Pantano, R. Woodman and J. Belcher, *J. Am. Cer. Soc.*, 2011, **94**, 2393.
20 J. M. Cole, E. R. H. van Eck, G. Mountjoy, R. Anderson, T. Brennan, G. Bushnell-Wye, R. J. Newport and G. A. Saunders, *J. Phys.: Condens. Matter*, 2001, **12**, 4105.
21 G. Mountjoy, J. M. Cole, T. Brennan, R. J. Newport, G. A. Saunders and G. W. Wallidge, *J. Non-Cryst. Solids*, 2001, **279**, 20.
22 J. M. Cole, E. R. H. van Eck, G. Mountjoy, R. J. Newport, T. Brennan and G. A. Saunders, *J. Phys. Condens. Matter.*, 1999, **11**, 9165.
23 R. Anderson, T. Brennan, J. M. Cole, G. Mountjoy, D. M. Pickup and R. J. Newport, *J. Mater. Res.*, 1999, **14**, 4706.
24 J. L. Rygel, Y. Chen, C. G. Pantano, T. Shibata, J. Du, L. Kokou, R. Woodman and J. Belcher, *J. Am. Cer. Soc.*, 2011, **94**, 2442.
25 A. Pedone, G. Malavasi, A. N. Cormack and M. C. Menziani, *Theor. Chem. Acc.*, 2008, **120**, 557.
26 G. Malavasi, A. Pedone and M. C. Menziani, *J. Phys. Chem. B*, 2013, **117**, 4142.
27 A. Tilocca, *J. Chem. Phys.*, 2008, **129**, 084504.
28 A. Tilocca, N. de Leeuw and A. N. Cormack, *Phys. Rev. B*, 2006, **73**, 104209.
29 G. Dick and A. W. Overhauser, *Phys. Rev.*, 1958, **112**, 90.
30 A. P. Rowley, P. Jemmer, M. Wilson and A. P. Madden, *J. Chem. Phys.*, 1998, **108**, 10209.
31 A. Aguado, L. Bernasconi, S. Jahn and A. P. Madden, *Faraday Discuss.*, 2003, **124**, 171.
32 R. I. Ainsworth, D. Di Tommaso, J. K. Christie and N. H. de Leeuw, *J. Chem. Phys.* , 2012, **137**, 234502.
33 C. Maltz, *Chem. Phys. Lett.*, 1969, **3**, 707.
34 L. Minervini, M. O. Zacate and R. W. Grimes, *Solid State Ionic*, 1999, **116**, 339.
35 T. X. T. Sayle, S. C. Parker and C. R. A. Catlow, *Surf. Sci.*, 1994, **316**, 329.
36 E. Gambuzzi, A. Pedone, M. C. Menziani, F. Angeli, D. Caurant and T. Charpentier, *Geochim. Cosmochim. Acta*, 2014, **125**, 170.
37 A. Pedone, E. Gambuzzi and M. C. Menziani, *J. Phys. Chem. C*, 2012, **116**, 14599.
38 A. Tilocca, A. N. Cormack and N. de Leeuw, *Chem. Mater.*, 2007, **19**, 95.
39 D. Di Tommaso, R. I. Ainsworth, E. Tang and N. De Leeuw, *J. Mater. Chem. B*, 2013, **1**, 5054.
40 J. K. Christie, R. I. Ainsworth, D. di Tommaso and N. H. de Leeuw, *J. Phys. Chem. B*, 2013, **117**, 10652.
41 K. P. Schroder, J. Sauer, M. Leslie, C. R. A. Catlow and J. M. Thomas, *Chem. Phys. Lett.* , 1992, **188**.
42 A. Pedone, G. Malavasi and M. C. Menziani, *J. Phys. Chem. C*, 2009, **113**, 15723.
43 J. Malik and A. Tilocca, *J. Phys. Chem. B*, 2013, **117**, 14518.
44 H. Barnighausen and G. Schiller, *J. Less-Common Metals*, 1985, **110**, 385.
45 R. W. G. Wickoff, *Crystal Structure*, 2nd edn., 1963.
46 M. Rzaigui, N. Kbir Ariguib, M. T. Averbuch-Pouchot and A. Durif, *J. Solid Chem.*, 1984, **52**, 61.
47 B. Deng and J. A. Ibers, *Acta Cryst.*, 2005, **61**, 76.
48 Y. Ni, J. M. Hughes and A. N. Mariano, *Am. Miner.*, 1995, **80**, 21.
49 T. M. Kato, *Neues Jahrbuch fur Mineralogie, Monatshefte*, 1990, **1990**, 227.
50 J. M. S. Skakle, C. L. Dickson and F. P. Glasser, *Powder Diffraction*, 2000, **15**, 234.
51 J. D. Gale, *Philos. Mag. B*, 1996, **73**, 3.
52 J. D. Gale, *J. Chem. Soc., Faraday Trans.*, 1997, **93**, 629.
53 J. E. Shelby, ed., *Introduction to Glass Science and Technology*, 1997 edn., The Royal Society of Chemistry, Cambridge.
54 P. S. Baram and S. C. Parker, *Philos. Mag. B*, 1996, **7**, 49.
55 A. Pedone, *J. Phys. Chem. C*, 2009, **113**, 20773.
56 W. Smith and T. R. Forester, *J Mol Graphics* 1996, **14**, 136.
57 A. I. Priven, *Glass Phys. Chem.*, 2001, **26**, 541.
58 V. K. Leko and O. V. Mazurin, *Glass Phys. Chem.*, 2003, **29**, 216.
59 A. I. Priven, *Glass Technol.: Eur. J. Glass Sci. Technol., Part A*, 2004, **45**, 244.
60 A. Pedone, T. Charpentier and M. C. Menziani, *Phys. Chem. Chem. Phys.*, 2010, **12**, 6054.
61 A. Pedone, T. Charpentier and M. C. Menziani, *J. Mater. Chem.*, 2012, **22**, 12599.
62 A. Pedone, E. Gambuzzi, G. Malavasi and M. C. Menziani, *Theor. Chem. Acc.* , 2012, **131**, 1147.
63 G. Mountjoy, *J. Non-Cryst. Solids*, 2007, **353**, 2029.
64 R. Dupree, D. Holland and M. G. Mortuza, *Nature*, 1987, **328**, 416.
65 M. E. M. Fleet, S. , M. Kasrai and S. Prabakar, *J. Non-Cryst. Solids*, 1997, **220**, 85.
66 V. Petkov, S. J. L. Billinge, S. D. Shastri and B. Himmel, *Phys. Rev. Lett.*, 2000, **85**, 3436.
67 A. C. Wright, A. G. Clare, B. Bachra, R. N. Sinclair, A. C. Hannon and B. Vessal, *Trans. Am. Crystallogr. Assoc.* , 1991, **27**, 239.
68 R. A. Martin, P. S. Salmon, H. E. Fischer and G. J. Cuello, *J. Non-Cryst. Solids*, 2004, **345–346**, 208.
69 D. I. W. Grimley, A. C. and R. N. Sinclair, *J. Non-Cryst. Solids*, 1990, **119**, 49.
70 G. S. Henderson, *J. Non-Cryst. Solids*, 1995, **183**, 43.
71 A. Pedone, G. Malavasi, M. C. Menziani, A. N. Cormack and U. Segre, *J. Phys. Chem. B*, 2006, **110**, 11780.
72 R. K. Brow, C. A. Click and T. M. Alam, *J. Non-Cryst. Solids*, 2000, **274**, 9.
73 M. Karabulut, E. Metwalli and R. K. Brow, *J. Non-Cryst. Solids*, 2001, **283**, 211.
74 R. Dupree, D. Holland, M. G. Mortuza, J. A. Collins and M. W. G. Lockyer, *J. Non-Cryst. Solids*, 1988, **106**, 403.
75 R. Dupree, D. Holland and M. G. Mortuza, *Phys. Chem. Glasses*, 1988, **29**, 18.
76 K. M. Wetherall, D. M. Pickup, R. J. Newport and G. Mountjoy, *J. Phys.: Condens. Mat.*, 2009, **21**, 035109.
77 D. M. Pickup, I. Ahmed, P. Guerry, J. C. Knowles, M. E. Smith and R. J. Newport, *J. Phys.: Condens. Mat.*, 2007, **19**, 415116.